Experiments in Fluids (2023) 64:24
https://doi.org/10.1007/s00348-022-03557-9

RESEARCH ARTICLE

Shear layers in two-stage compound channels investigated with LS-PIV

Victor Dupuis[1] · Laura Schraen[1] · Olivier Eiff[1]

Received: 30 September 2022 / Revised: 9 December 2022 / Accepted: 20 December 2022

Abstract
Flow experiments are conducted in a two-stage compound open-channel, with varying intensity of the velocity difference between the main channel (deep part) and the floodplain (shallower part), using a large-scale free surface PIV technique (LS-PIV). For all investigated flows, a shear layer develops at the interface between main channel and floodplain, characterised by a peak of turbulent shear stress. Yet, two different kinds of shear layer could be identified. The first kind is characterised by the presence of large-scale quasi-periodic structures of Kelvin-Helmholtz type which are growing in downstream direction, whereas the second kind is characterised by smaller-scale vortical structures without quasi-periodicity and which do not grow in downstream direction. The shear parameter $\lambda = (U_2 - U_1)/(U_2 + U_1)$, where U_1 and U_2 are defined as the velocities outside the shear layer, is identified as a key parameter to distinguish between these two types of shear layers, supporting a result from Proust et al. (Water Resour Res 53: 3387–3406, 2017). A physical interpretation of the λ-criterion is proposed, based on the inhibiting effect of ambient turbulence (the turbulence level outside the shear layer) on the emergence of Kelvin-Helmholtz structures. Accordingly, the threshold value of λ, above which large-scale structures can develop, is dependent on the level of the ambient turbulence. Despite their very different behaviours, the two types of shear layer have the same efficiency to generate turbulent shear stress for a given velocity difference across the shear layer, except for λ-values close to the threshold value.

1 Introduction

The flow in a two-stage compound channel, consisting of a cross section having two levels, is a canonical flow which has been studied since at least the 1960s (Sellin 1964) in the context of understanding and modelling the flow in overflowing rivers.

The main particularity of the two-stage compound channel is the shear layer which develops between the deep part (the main channel) and the shallower part (the floodplain). This shear layer can in a first approach be analysed with the theory which was developed for the plane mixing layer, another canonical flow. But while similarities exist between the compound channel shear layer and the plane mixing layer (namely a time-averaged velocity profile with an inflection point, a widening in streamwise direction, self-similarity of the profiles of velocity and turbulence, as well as the presence of large-scale structures of Kelvin-Helmholtz type), important differences also prevail. The compound channel flow is confined vertically by the bed and the free surface, and laterally by the side walls. Its time-averaged flow is therefore strongly 3D and asymmetric, whereas the time-averaged flow of the plane mixing layer is by definition 2D and is antisymmetric at a given streamwise position. In addition, the friction on the bed and the presence of side walls limit the width of the shear layer (Chu and Babarutsi 1988; Dupuis et al. 2017; Proust and Nikora 2020), contrary to the plane mixing layer which grows indefinitely. Finally, whereas the plane mixing layer is a boundary-free flow for which the single source of turbulence is the internal shear, the compound channel flow experiences a supplementary source of turbulence through the boundary layer on bed and walls.

Under uniform flow conditions, the intensity of the compound channel shear layer decreases with the relative depth $D_r = h_f/h_m$, where h_f is the water depth in the floodplain and h_m the water depth in the main channel. According to Stocchino and Brocchini (2010), for $D_r > 0.5$, there is nearly no

✉ Victor Dupuis
victor.dupuis@kit.edu

[1] Karlsruher Institut für Technologie, Karlsruhe, Germany

Published online: 24 January 2023

shear layer any more, and the behaviour of the flow tends to the one in a rectangular channel.

Kelvin-Helmholtz large-scale structures are often present in compound channel shear layers, but not always. The issue concerning the conditions under which these structures appear was addressed by Proust et al. (2017), who found that Kelvin-Helmholtz structures are observed only when $\lambda > 0.3$, where λ is the shear parameter defined by $\lambda = (U_2 - U_1)/(U_2 + U_1)$ with U_2 and U_1 being velocity scales characterising the high-speed side and the low-speed side of the shear layer, respectively.

The aim of the present study is to confirm if there is, as the criterion proposed by Proust et al. (2017) suggests, a threshold effect concerning the presence of Kelvin-Helmholtz type structure in a compound channel shear layer, or in other words, if there is a critical value of λ above which these structures are present and under which they are not existent. Further, we want to characterise more precisely what distinguishes physically shear layers with and without these structures.

As the Kelvin-Helmholtz type structures are very large (typically on the order of the channel width), a large-scale measurement technique appeared suitable, which would capture the whole velocity field of the structures and be able to follow their downstream evolution. To this end, a large-scale surface PIV system was set up, which allowed the velocity field at the free surface to be recorded over a longitudinal distance of six times the channel width.

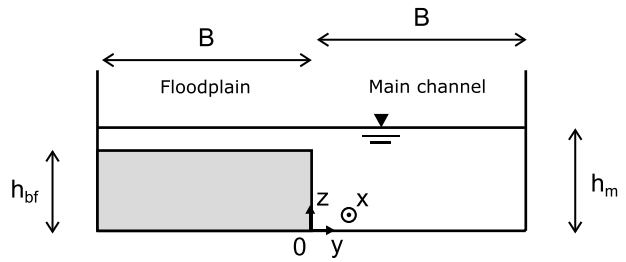

Fig. 1 Cross-sectional view of the experimental channel (looking from downstream)

2 Experimental method

The experiments were conducted in a 20 m long open-channel glass-wall flume at the Institute for Hydromechanics of the KIT in Karlsruhe, Germany. The flume has a width of $2B = 80$ cm and an adjustable slope, which was set to $S_0 = 0.5$ mm.m^{-1}. A two-stage compound section, as sketched in Fig. 1, was built, with half of the channel section being a floodplain made of PVC and of height $h_{bf} = 15$ cm (bankfull level).

At the inlet of the channel, a ramp of 1.3 m length on the floodplain side raises the water on the bankfull level (see Fig. 2). The two subsections are first separated by a splitter plate, which ends 0.3 m downstream of the ramp. The two subsections are fed by the same inlet tank, upstream of the splitter plate, where grids and honeycombs are placed to homogenise the flow.

The longitudinal axis x follows the channel bed and has its origin at the trailing edge of the splitter plate. The lateral axis y is oriented from the floodplain to the main channel with origin at the interface between the two (Fig. 1). The vertical axis is normal to the bed with origin at the bottom of the main channel. The velocities in these three directions are denoted u, v and w and an overbar indicates a time-average. h_m denotes the water depth in the main channel and $h_f = h_m - h_{bf}$ is the water depth in the floodplain.

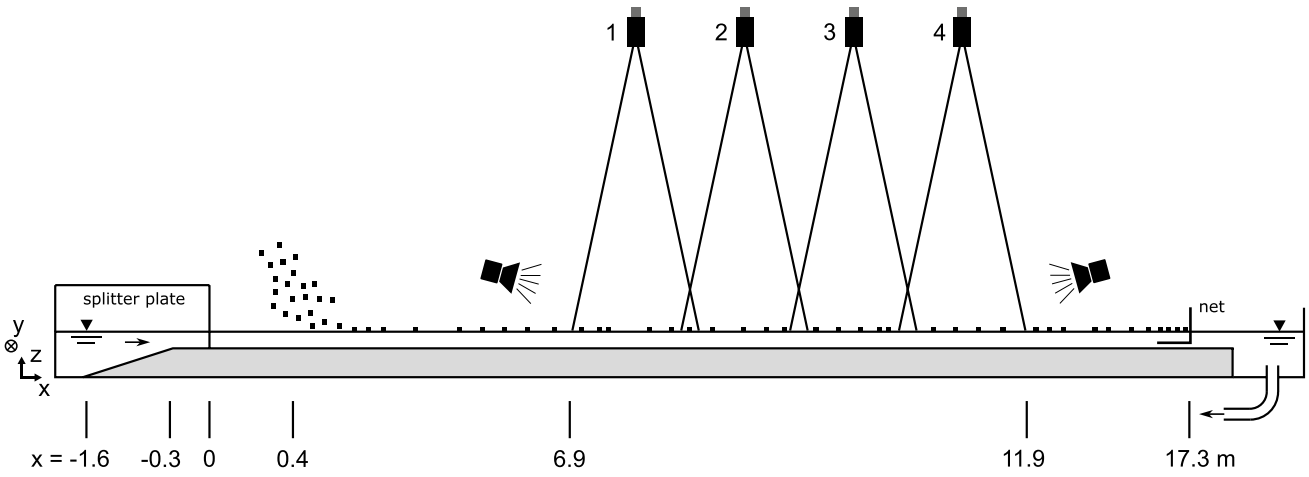

Fig. 2 Sketch of the LS-PIV set-up (not at scale). The two subsections are separated by a splitter plate till $x = 0$. The particles are seeded at $x \approx 0.4$ m and are gathered back at $x = 17.3$ m in a net

Contrary to most laboratory flumes, the present flume does not have a weir with a free water fall at the outlet. The water exits the flume at the downstream end through an outlet tank and a pipe (Fig. 2). The flow in the channel is therefore controlled by the slope, the discharge, and the amount of water in the system.

The velocity field at the free surface was measured using a multi-camera large-scale Particle Image Velocimetry technique (LS-PIV). LS-PIV consists in seeding the water surface with floating particles and to record the displacement of the particles with a camera (Fujita et al. 1998; Weitbrecht et al. 2002). The processing of the velocity vector field from the camera image follows the same principle as for classical PIV.

One of the most delicate technical issue with LS-PIV is to find particles that do not agglomerate. Most of the particles have the tendency to build groups after a short time, which makes the measure impossible. As brought out by Vella and Mahadevan (2005), the attraction between particles can be explained by the gravity and buoyancy forces that act on the particles placed at the deformed free surface. Thus, although surface tension plays a key role – along with gravity and buoyancy – in the local free surface deformation around the particle, it is not directly the surface tension force which makes particles attract together. To avoid attraction, one way is therefore to avoid free surface deformation. After trying several particle materials and shapes, we found that the best results were obtained with pieces of polypropylene foil. The particles were cut from a gift ribbon (of yellow or white colour), to make squares of 5 mm side. A single particle is so flat and light that the free surface deformation around it is minimal.

In order to have a large measurement field with good spatial resolution, four cameras were installed side-by-side, each camera having a field of view of approximately 1.25 m, as is sketched in Fig. 2. In this way, a region of five metres long, from $x = 6.9$ m to $x = 11.9$ m, and spanning the whole width of the channel could be covered by the measurement. The cameras (IDS UI-3180CP of resolution 2592×2048 px^2 for cameras 1 and 4 and IDS UI-3060CP of resolution 1936×1216 px^2 for cameras 2 and 3) were installed at approximately 2.5 m above the water surface with objectives of 25 mm (Lensation Lensagon CHS25095) for camera 1 and 4 and of 24 mm (Sigma 24/1.8 EX DG Macro) for camera 2 and 3. The four cameras were synchronised with a common trigger. The spatial resolution was 2.15 px.mm^{-1} for cameras 1 and 4 and 1.47 px.mm^{-1} for cameras 2 and 3. The free surface was illuminated by two projectors, one upstream and one downstream of the measurement section, placed such that light reflections are avoided.

Images were recorded continuously with a frequency ranging from 25 to 75 Hz, depending on the flow velocity. The particles were seeded by hand at $x \approx 0.4$ m and were collected by a net at the downstream end of the flume. This net consisted of a stainless steal grid of very thin wires in order to minimise flow resistance. Due to accumulation of particles in the net, the measurement time was limited to approximately two minutes for each flow test case, in order to not affect the subcritical flows by altered downstream conditions.

The images were processed with the commercial software Davis10 from LaVision. In this software the cross-correlation is implemented with FFT and the estimation of sub-pixel displacement is based on a three-point estimator, the correlation peak being fit with a Gaussian function. An adaptative mask (i.e. a specific mask for each image) was used, in order to remove regions without or with not enough particles. The adaptative mask was generated by a MATLAB program based on an erosion filter. A multipass processing was applied, with the final pass having a box size of 96×96 px^2 and an overlap of 50 %. This results in a spatial resolution of the velocity field of 22.3 mm (in both x- and y-direction) for cameras 1 and 4 and 32.5 mm for cameras 2 and 3. This relative coarse spatial resolution does not allow to resolve the small-scale turbulence, such that it has to be expected that the kinetic energy is slightly truncated.

Eight flow test cases were investigated, whose flow conditions are presented in Table 1. The test cases vary in relative depth $D_r = h_f/h_m$ and in bulk Reynolds number $Re_Q = U_Q R_h/\nu = Q/(P_w \nu)$, where Q is the discharge, $U_Q = Q/A$ the bulk velocity, A the channel cross section, $R_h = A/P_w$ the hydraulic radius, P_w the wetted perimeter and ν the kinematic viscosity.

Since the relative depth D_r is related to the shear parameter λ but the latter is more physically relevant, as will be shown in the following, the test cases are named according to the shear parameter and the Reynolds number. The shear parameter λ was calculated from the lateral profile of velocity, presented later in Section 5. As λ varies with x, the values at $x = 7.5$ m and $x = 11.5$ m within the measurement zone are reported in Table 1.

There are three flow test cases with a high shear parameter $\lambda > 0.45$ (HighA, HighB and HighC, where the letters A, B C denotes increasing Reynolds numbers), two test cases with a low shear parameter $\lambda < 0.2$ (LowA and LowB) and three flow test cases with an intermediate shear parameter $0.2 < \lambda < 0.45$ (Inter1 having higher λ-values than Inter2A and Inter2B).

The water depth increased in downstream direction for each test case, implying that the flows were globally decelerating. The longitudinal gradient of the flow depth, reported in the last column of Table 1, was always smaller than the slope of the channel S_0 and the variation of the floodplain flow depth h_f was of maximum 8 % within the measurement section ($6.9 < x < 11.9$ m). This slight non-uniformity is not expected to affect sensitively the dynamics of the shear

Table 1 Flow conditions of the test cases. h_f is the water depth in the floodplain (here at $x = 9.5$ m), $D_r = h_f/h_m$ the relative depth, Q the discharge, $U_Q = Q/A$ the bulk velocity with A the channel cross section, $Re_Q = U_Q R_h/\nu$ the bulk Reynolds number with R_h the hydraulic radius, λ is the shear parameter, whose value is given both at $x = 7.5$ m and $x = 11.5$ m and $\frac{1}{S_0}\frac{dh}{dx}$ is the mean longitudinal gradient of water depth normalised by the channel slope

Test case	h_f mm	D_r	Q L.s^{-1}	U_Q m.s^{-1}	$Re_Q \times 10^3$	λ $x = 7.5$ m	λ $x = 11.5$ m	$\frac{1}{S_0}\frac{dh}{dx}$
HighA	20	0.118	8.0	0.105	7.0	0.45	0.45	0.77
HighB	19	0.112	16.7	0.222	14.7	0.51	0.51	0.65
HighC	19	0.112	25.7	0.342	22.6	0.55	0.52	0.52
Inter1	24	0.138	25.0	0.316	21.8	0.30	0.44	0.26
Inter2A	31	0.171	13.4	0.158	11.5	0.24	0.36	0.65
Inter2B	33	0.180	24.5	0.284	21.0	0.19	0.30	0.39
LowA	46	0.235	13.8	0.143	11.6	0.11	0.19	0.90
LowB	46	0.235	26.0	0.269	21.8	0.10	0.15	0.65

layers investigated. For comparison, Kironoto and Graf (1994) and Song and Chiew (2001) show that for a rectangular open-channel flow, non-uniformities of the water surface up to one time the energy slope do not change qualitatively the turbulence structure of the flow.

Right after the splitter plate, a lateral bulk flow between floodplain and main channel occurs, as the discharge distribution between these two sections is in imbalance. According to Bousmar et al. (2005), a streamwise distance of at least $35B_f$, where B_f is the floodplain width, is necessary to achieve a mass balance between main channel and floodplain. The measurement section in the present investigation starts $17B_f$ downstream of the splitter plate, such that a mass imbalance due to the inlet conditions may remain. Yet, the lateral time-averaged velocities were very weak in the measurement region ($\overline{v}/U_Q$ is maximum about 3 %), such that lateral mass transfer is not expected to affect significantly the flow dynamics. It should also be considered that mass redistribution between main channel and floodplain is not due solely to the inlet conditions, but can be a natural consequence of the development of the shear layer between main channel and floodplain. This latter mass transfer, which always occurs towards the floodplain, is usually very weak and is analogous to the deviation of the plane mixing layer towards the low-speed side (Yule 1972).

3 Time-average analysis

The left column of Fig. 3 shows the time-averaged longitudinal velocity normalised by the bulk velocity, $\overline{u}/U_Q$, for the eight test cases. At first sight there seems to be no fundamental difference between these different flows: there is a high-speed flow in the main channel, a low-speed flow on the floodplain and a zone with intermediate velocity between the two. We can nevertheless observe some differences between the flows with high and with low shear parameter λ: the formers (HighA, HighB and HighC) feature a noticeable longitudinal evolution, the zone with intermediate velocity becoming wider downstream; for the latter on the contrary (LowA and LowB), there is no widening of the region of intermediate velocity, the only noticeable evolution is a velocity decrease in the floodplain (region $y < 0$).

A simple calculation shows that this velocity decrease in the floodplain for the low-λ cases can not be attributed to the increase in water depth. It is therefore due to a transfer of fluid towards the main channel. This mass transfer is clearly due to mass imbalance at the channel inlet, which takes a lot of streamwise distance to dissipate, as explained above.

The lateral turbulent shear stress at the free surface normalised by the bulk velocity, $-\overline{u'v'}/U_Q^2$, is shown in the right column of Fig. 3 for all test cases. All cases feature a region of high turbulent shear stress away from the walls, which therefore do not correspond to boundary layer turbulent shear stress. These zones of high turbulent shear stress are called in the following shear layers. A significant difference in intensity of $-\overline{u'v'}/U_Q^2$ in the shear layer can be identified between the cases with high and with low shear parameter: for high λ, the maximum of $-\overline{u'v'}/U_Q^2$ is on the order of 4.10^{-3}, and on the order of 4.10^{-4} for low λ. For the latter, the turbulent shear stress in the shear layer is of the same order of magnitude (but of opposite sign) than the wall turbulent shear stress at the left wall (blue region on the top).

A second difference is the position of the shear layer: while for the cases with high λ the shear layer is located slightly towards the floodplain (maximum of shear in the range $y = -0.06$ to -0.03 m), the shear layer for the flows with low λ lies within the main channel (maximum of shear in the range $y = 0.08$ to 0.12 m). A third difference, which supports what was observed for $\overline{u}$, concerns the longitudinal development: for the flows with high λ, the shear layer is widening in downstream direction, whereas for the ones with low λ, the width of the shear layer stays quite constant.

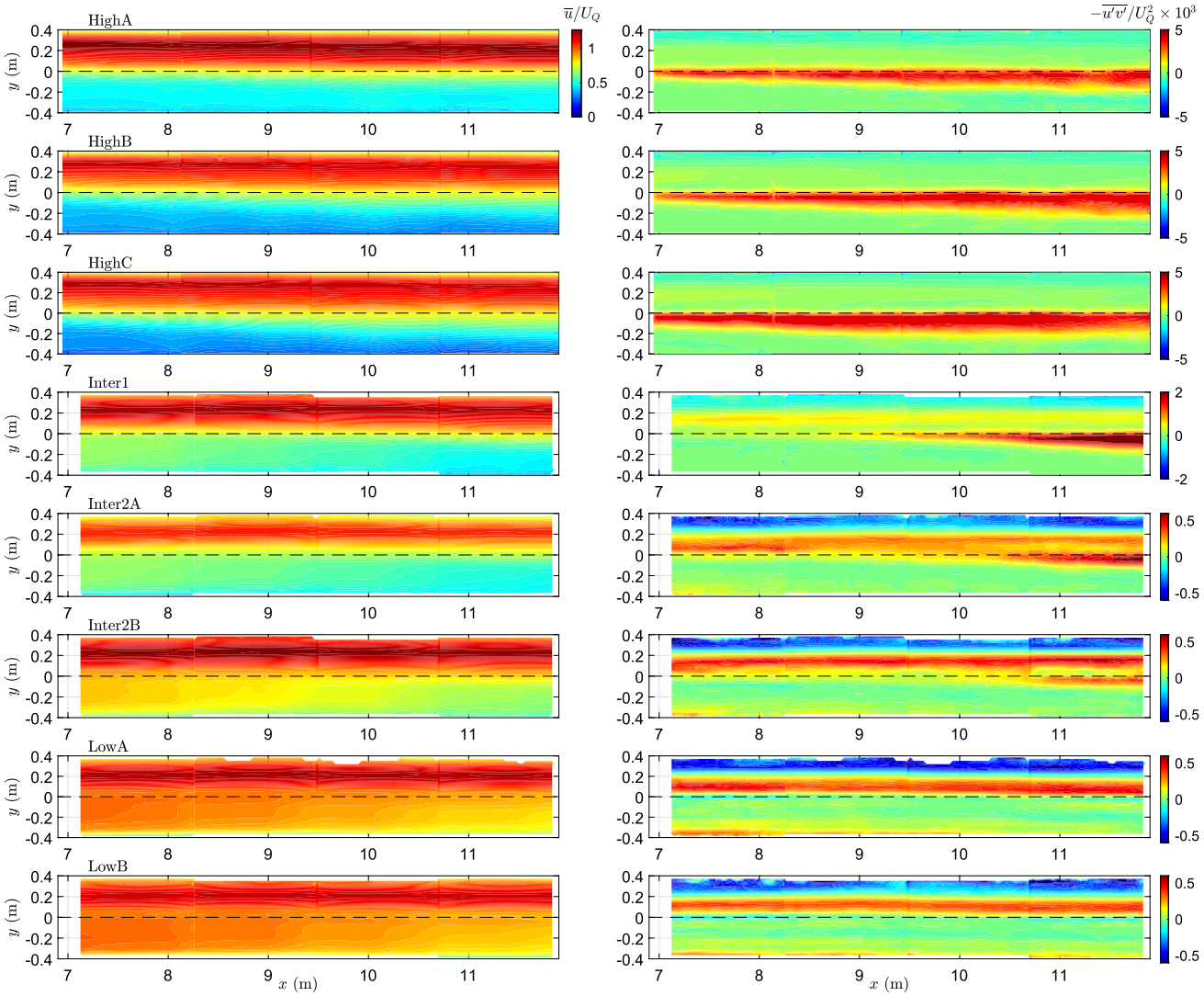

Fig. 3 Left column: Longitudinal time-averaged velocity normalised by the bulk velocity, $\overline{u}/U_Q$, at the free surface for the eight test cases; the color-scale is the same for all panels. Right column: Lateral turbulent shear stress normalised by the bulk velocity, $-\overline{u'v'}/U_Q^2 \times 10^3$, at the free surface for the eight test cases; the color-scale is not the same for the different panels

As for the test cases with intermediate λ, it can be seen that the value of $-\overline{u'v'}/U_Q^2$ in the shear layer is also intermediate. More surprisingly, the two types of shear layer described above (for high and for low λ) are present concomitantly downstream of the measurement region. For all these three cases (Inter1, Inter2A and Inter2B), a low-λ-type shear layer exists all along the field of view, centred at approximately $y = 0.15$ m, but additionally a high-λ-type shear layer begins to develop at $x \approx 10$ m, and is rapidly widening.

It therefore appears that, depending on the shear parameter λ, two different kinds of shear layer can develop at the interface between main channel and floodplain, and that for some cases, these two kinds of shear layers can even coexist. In the following we want to determine more precisely what distinguishes these two types of shear layer.

4 Large-scale structures

Figure 4 shows two instantaneous velocity vector fields $(u - U_r, v)$, for the test cases HighC and LowB. U_r is a constant convection velocity, taken as the longitudinal velocity at the position of the maximum turbulent shear stress, the location where large-scale structures are expected. Also plotted is the Q-quantity, which is often used as a criterion to detect vortices (Epps 2017). Approximating the free surface flow as 2D, the Q-quantity (named in this way to distinguish

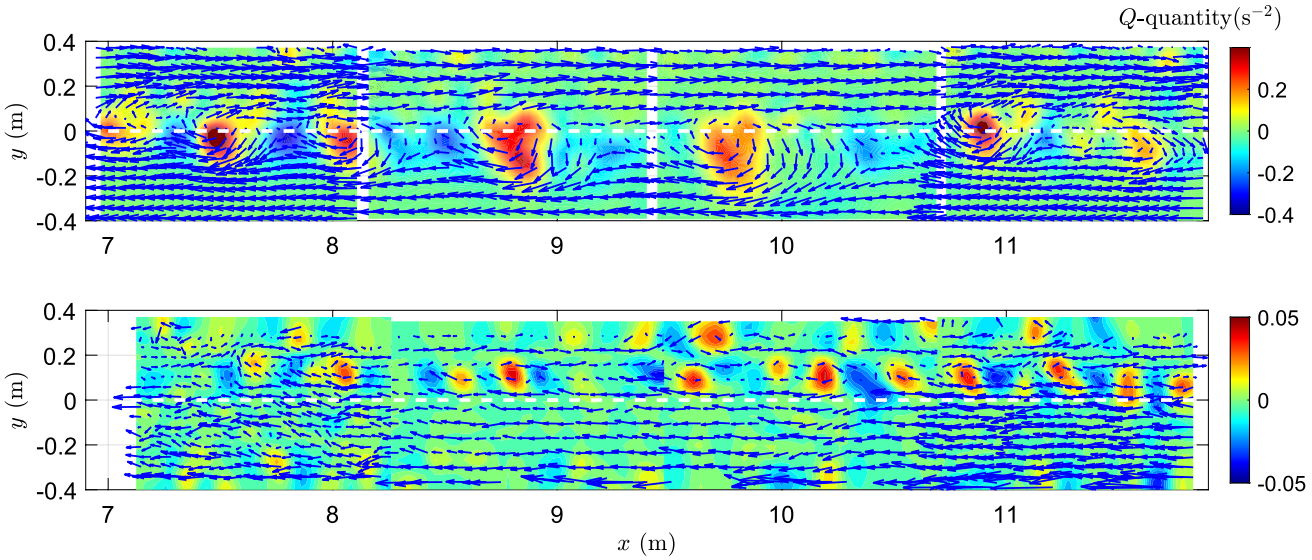

Fig. 4 Instantaneous velocity field $(u - U_r, v)$ at the free surface together with the Q-quantity in the background for test case HighC (*top*) and LowB (*bottom*). Only one vector over four is drawn. U_r is a constant velocity, equal to the longitudinal velocity at the position of the maximum turbulent shear stress

from the discharge) reduces to the determinant of the Jacobian matrix: $Q\text{-quantity} = \partial u/\partial x \; \partial v/\partial y - \partial u/\partial y \; \partial v/\partial x$.

For HighC, large vortices can be observed, regularly spaced, separated by saddle points, and located at the same lateral position as the zone of maximum turbulent shear stress. These patterns can be clearly identified as the Kelvin-Helmholtz structures that appear in turbulent plane mixing layers (e.g. Loucks and Wallace 2012). For test case LowB, vortices can be detected too, and they are also located at the region of maximum turbulent shear stress. Yet, they are much smaller and less regularly spaced as in the precedent case.

In order to confirm these qualitative observations made on the instantaneous flow field, a two-point spatial correlation of the longitudinal velocity, $R_{uu}(x, y)$, is carried out for the same two flows. To evaluate the longitudinal evolution, the reference point for the correlation was set first at $x = 7.8$ m and then at $x = 11.1$ m (and laterally at the y-position of the maximum turbulent shear stress). The results are presented in Fig. 5 for HighC and Fig. 6 for LowB. For HighC, the spatial correlation features a damped periodic pattern, which indicates the presence of quasi-periodic large-scale structures. This pattern is growing between $x = 7.8$ m and $x = 11.1$ m, stating that the large-scale structures are growing in size too. For LowB, the region of high spatial correlation is much smaller, much more isotropic and does not grow in size in downstream direction. Furthermore, no periodicity is observed. The absence of quasi-periodicity suggests that the vortices that were observed in the instantaneous flow field for LowB are not of Kelvin-Helmholtz type, or at least that they could not arrange in a train of quasi-periodic vortices.

The pattern of the spatial correlation map for HighC is particularly skewed, forming two branches starting from the interface: one going towards the floodplain with an angle of approximately 45° and the other one going towards the main channel with a much steeper angle of about 70° (with reference to the lateral axis). A similar skewing of the spatial correlation was obtained by Dupuis (2016) in compound channels with rough floodplains. The reason of this shape is not clear. The coherence of the structures extends over all the floodplain width, as was already observed by Dupuis (2016) and Proust and Nikora (2020). This suggests that for flows with high λ, the floodplain vertical wall is the limitation factor for the lateral extension of the coherent structures. On the main channel side however, the coherence is rapidly lost.

5 Shear layer characteristics

For laminar flows, the theorem of Fjortoft establishes mathematically that the presence of an inflection point in the velocity profile is a necessary condition for the Kelvin-Helmholtz instability to develop (see e.g. Huerre and Rossi 1998). The theorem of Fjortoft also requires that at the inflection point $\partial\overline{u}/\partial y \; \partial^3\overline{u}/\partial y^3 < 0$, which means that the velocity profile passes from a convex shape to a concave shape through the inflection point, when going in the direction of increasing velocity. On the contrary, inflection points for which the velocity profile passes from a concave to a convex shape in the direction of increasing velocity

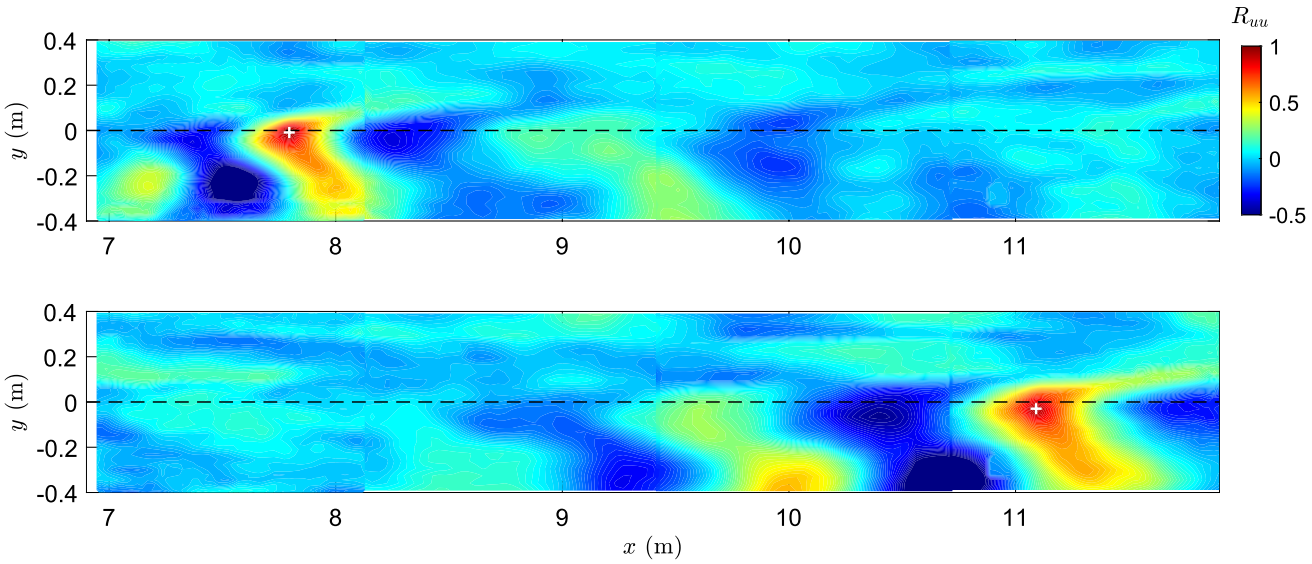

Fig. 5 Two-point spatial correlation for longitudinal velocity u for test case HighC with reference point at $x = 7.8$ m and $y = 126$ mm (*top*) and at $x = 11.1$ m and $y = 102$ mm (*bottom*). The location of the reference point is indicated by a white cross

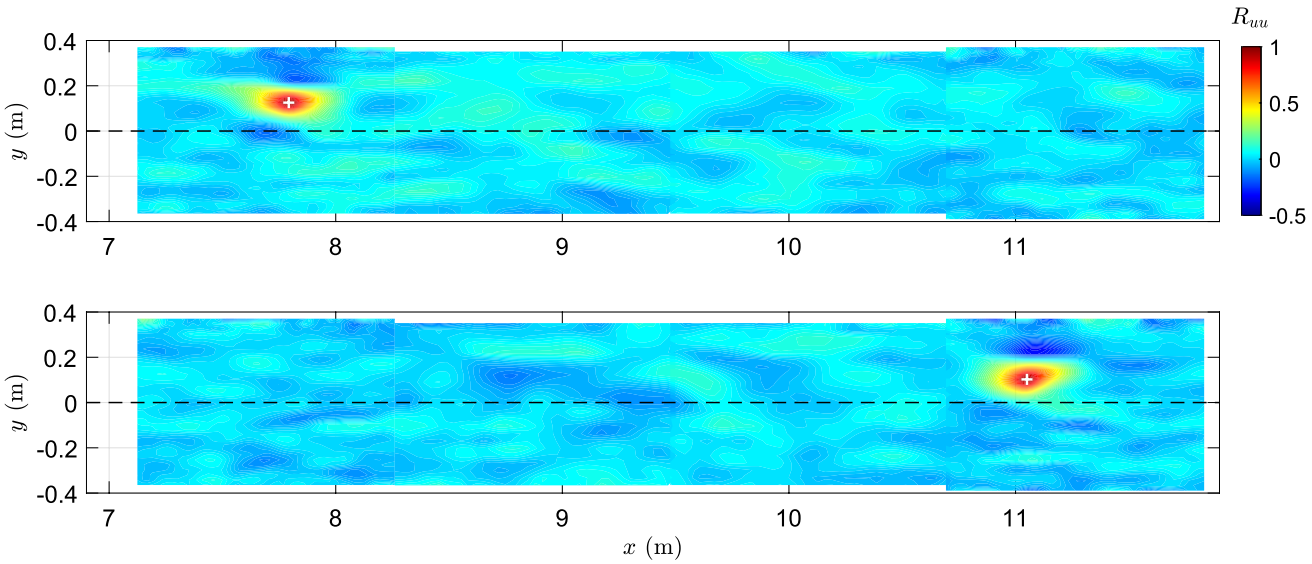

Fig. 6 Two-point spatial correlation for longitudinal velocity R_{uu} for test case LowB with reference point at $x = 7.8$ m and $y = -9$ mm (*top*) and at $x = 11.1$ m and $y = -30$ mm (*bottom*). The location of the reference point is indicated by a white cross

are stable. For turbulent flows no such theorem exists to our knowledge. It is not known if either the time-averaged velocity profile or the instantaneous velocity profile needs to have an inflection point for Kelvin-Helmholtz structures to develop. What the broad literature on plane turbulent mixing layers however shows, is that the position of the maximum of turbulent shear stress, and by deduction the centre of the Kelvin-Helmholtz structures, coincides or is very close to the inflection point of the mean velocity profile (Bell and Mehta 1990; Olsen and Dutton 2002; Loucks and Wallace 2012). Dupuis et al. (2017) and Proust et al. (2022) found for shear layers in two-stage and rectangular channels respectively, again that the position of the inflection point and of the peak of turbulent shear stress nearly always coincide or are very close.

Figure 7a shows the lateral profile of the time-averaged longitudinal velocity at $x = 11.5$ m for each test case, with the position of inflection points indicated by circles. To find the inflection points, the velocity profiles were previously slightly smoothed (but Fig. 7a shows the non-smoothed profiles). Only inflection points fulfilling Fjortoft's criterion are depicted.

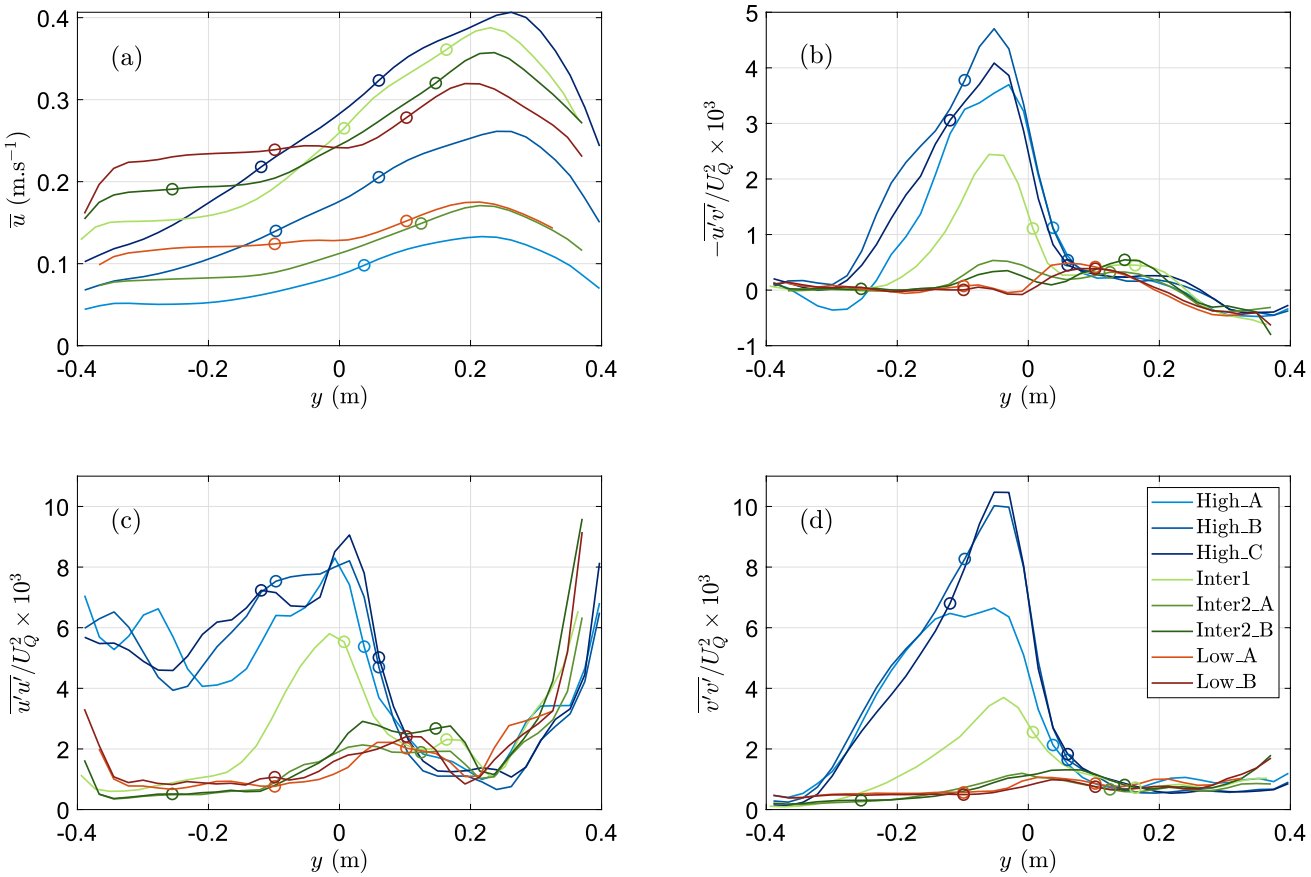

Fig. 7 Lateral profiles of normalised longitudinal velocity **a**, normalised lateral turbulent shear stress **b**, normalised longitudinal turbulence intensity **c** and normalised lateral turbulence intensity **d** at $x = 11.5$ m for all flow cases. The circles denote the positions of the inflection points of the velocity profile (only the ones fulfilling Fjortoft's criterion)

Except for HighA and Inter2A, which have only one inflection point (both located in the main channel), all other profiles have two inflection points, generally one located in the floodplain and the other one in the main channel. Only Inter1 has its two inflection points in the main channel. The uncertainty in the position of the inflection point was estimated as less than the spatial resolution (22 mm). In fact, one of the measurement (Inter1) was repeated twice, and the two infection points were found at the same position (within the accuracy of the spatial resolution).

The lateral profiles of turbulent shear stress at the same x-position as in Fig. 7a are plotted in Fig. 7b, where the positions of the inflection points of the velocity profiles are included. It can be observed that if the peaks of turbulent shear stress are often not far from an inflection point, the lag between the two is quite important. These observations therefore disagree with what is observed for plane mixing layers as well as for shear layers in channels for which, as mentioned above, inflection point and maximum turbulent shear stress were found to be very close to each other. A most probable explanation for this fact, but which could not be checked directly, is the influence of the splitter plate wake. The latter has probably not completely dissipated and still affects the shape of the velocity profile by generating a velocity defect. For the two cases LowA and LowB, a slight velocity dip can even be observed at $y \approx 0$ (Fig. 7a). The significant influence of the splitter plate wake in plane mixing layer experiments was identified by Bell and Mehta (1990) and was confirmed for shallow shear layer experiments by Proust et al. (2022). A second explanation, which may combine with the precedent, is the influence of secondary currents, which are known to affect significantly the momentum distribution within the cross section (Nezu and Nakagawa 1993). In any case, it would suggest that a small perturbation of the velocity profile (either due to a residual of the splitter plate wake or due to secondary currents) is enough to generate a significant lag between the position of the turbulent shear stress peak and the inflection point.

The profiles of longitudinal and lateral turbulence intensities, plotted in Fig. 7c-d, shows that the peak position of these quantities and the position of the turbulent shear stress peak do not coincide either. The maximum of turbulent shear

stress is located within the floodplain (Fig. 7b), while the maximum of longitudinal turbulence intensity is close to the interface at $y = 0$ (Fig. 7c). This difference in peak position for the different turbulent quantities is not observed for plane mixing layers. It must have its origin in the three-dimensionality of the flow, but further investigations are needed to better understand this fact.

For each flow, the shear parameter $\lambda = (U_2 - U_1)/(U_2 + U_1)$ was calculated locally from the lateral profile of velocity both at $x = 7.5$ m and at $x = 11.5$ m. U_2 was taken as the maximum velocity in the main channel and U_1 either as the velocity at the point where the velocity goes from the concave shape due to the wall boundary layer to the convex shape of the shear layer (this is an inflection point which does not fulfil Fjortoft's criterion) and which sometimes corresponds to a plateau region of the velocity in the floodplain, or as the velocity in the velocity dip if there is one (for LowA and LowB).

Inspection of the instantaneous velocity fields of the different flow cases (as in Fig. 4) shows that for all cases for which Kelvin-Helmholtz type structures are clearly present, i.e. for the three High-cases and for Inter1 at 11.5 m, we have $\lambda > 0.3$. Inversely for the cases where these structures seem absent, i.e. for Inter2A at 7.5 m, Inter2B at 7.5 m, and for the two Low-cases, we have $\lambda < 0.3$. Moreover, at $\lambda \approx 0.3$, there is one case for which Kevin-Helmholtz structures just begin to appear (Inter2B at $x = 11.5$ m) and one case where they are absent (Inter1 at $x = 7.5$ m). The criterion suggested by Proust et al. (2017) mentioned in the Introduction is therefore confirmed by the present results.

Figure 8a shows the maximum of turbulent shear stress across the shear layer, $\max(-\overline{u'v'})$, normalised by the mean velocity $U_0 = (U_2 + U_1)/2$, as a function of the shear parameter λ. The values both at $x = 7.5$ m and at $x = 11.5$ m are reported. For the cases where there are two shear layers concomitant, the one with the highest turbulent shear stress was chosen. The quantity $\max(-\overline{u'v'})/U_0^2$ is strongly correlated to the shear parameter. For $\lambda < 0.3$, it is quite constant and equal to $(0.45 \pm 0.1) \times 10^{-3}$. Then a steep increase is observed for $\lambda > 0.4$ with a change of the order of magnitude, reaching 7.7×10^{-3} for $\lambda = 0.55$. These values are very close to the one measured by Proust et al. (2022) in the case of shear layers in a rectangular channel.

When the maximum of turbulent shear stress is normalised by the velocity difference $U_2 - U_1$, as shown in Fig. 8b, a completely different result appears (note that there is a factor $1/\lambda^2$ between the quantities plotted in the Fig. 8a and b). The quantity $\max(-\overline{u'v'})/(U_2 - U_1)^2$ reaches similar values for the lowest and highest λ, whereas around $\lambda = 0.3$, i.e. in the transition region between the two shear layer types, the values are 3-4 times lower. It seems therefore that, for a given velocity difference, the two types of shear layers are as effective for generating a turbulent

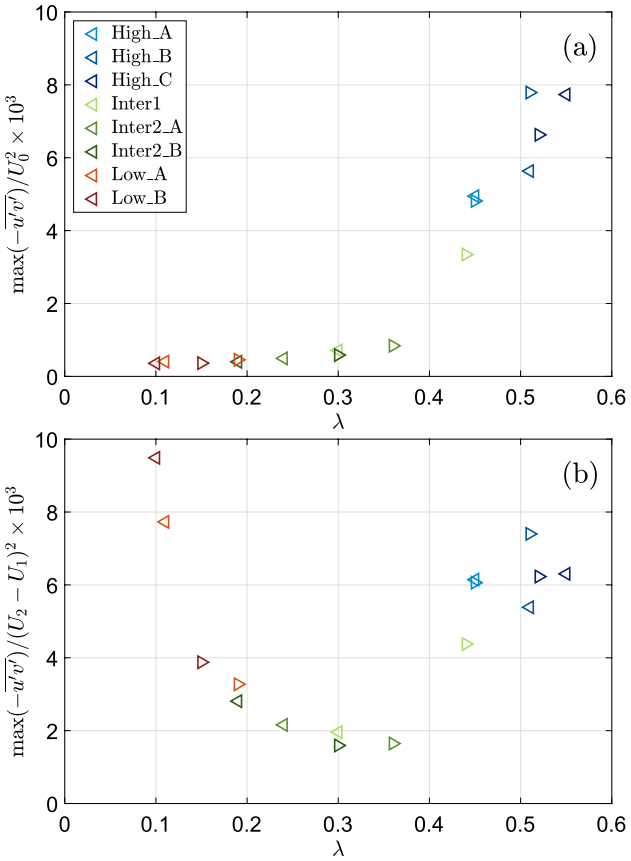

Fig. 8 Maximum of turbulent shear stress across the shear layer, $\max(-\overline{u'v'})$, normalised by the mean velocity $U_0 = (U_2 + U_1)/2$ **a** and by the velocity difference $U_2 - U_1$ **b**, as a function of the shear parameter λ. The symbols $\triangleleft$ refers to the values at $x = 7.5$ m and the symbols $\triangleright$ to the values at $x = 11.5$ m

shear stress. It is only the mechanism of the turbulence which is different. In the region $\lambda \approx 0.3$, however, the shear layer is less effective to generate turbulent shear stress.

Figure 9 shows the quantity $\max(-\overline{u'v'})/(U_2 - U_1)^2$ as a function of the Reynolds number. No correlation can be observed, such that the Reynolds number seems not to be an influential parameter for the maximum of turbulent shear stress. A similar result is obtained when normalising the maximum shear stress by the mean velocity U_0.

Note that the shear parameter λ should be seen as a macroscopic parameter characterising the shear layer, and not as a local parameter as is for example the turbulent viscosity. The point 1 and 2, where the velocity U_1 and U_2 are calculated, are at the edges of the shear layer. This edge is not always obvious to define, but it can be considered for example as the region from which another flow process becomes dominant (for example a wall boundary layer). If the points 1 and 2 would be chosen such that they

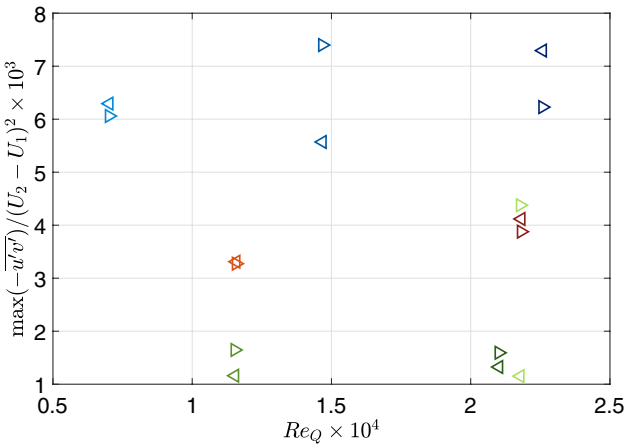

Fig. 9 Normalised maximum of turbulent shear stress across the shear layer, $\max(-\overline{u'v'})/(U_2-U_1)^2$, as a function of the bulk Reynolds number Re_Q. The symbols are the same as in Fig. 8

tend to each other, then the value of λ would tend to zero, confirming that λ is not a local parameter.

6 Discussion on the effect of ambient turbulence

An interpretation of the λ-criterion was proposed by Proust and Nikora (2020), who suggested that λ can be seen as the square root of the ratio of the turbulence energy associated with the Kelvin-Helmholtz structures to the energy associated with boundary layer turbulence from the bed. This interpretation can be extended in the following way. $U_2 - U_1$ can be considered as the typical velocity fluctuation associated with the Kelvin-Helmholtz structures. But if the ambient turbulence of the flow, meaning the level of turbulence outside the shear layer, already induces fluctuations of this order of magnitude, then the forming Kelvin-Helmholtz structures are disintegrated by the ambient turbulence and will at the best exist for very short life-times. If we consider that the ambient turbulence is proportional to the mean flow velocity $U_0 = (U_2 + U_1)/2$, i.e. $u_{\mathrm{rms}} \approx KU_0$, with K a constant, then it can be postulated that Kelvin-Helmholtz structures will only be viable if $U_2 - U_1 > K'u_{\mathrm{rms}}$, with K' another constant, or

$$\lambda > \lambda_{\mathrm{crit}} = \frac{K'K}{2}. \tag{1}$$

For shear layers in open-channel flows we have obviously $\lambda_{\mathrm{crit}} \approx 0.3$ and taking $K \approx 0.1$ (for a boundary layer for example, 10 % turbulent intensity is a commonly used value), it yields $K' \approx 6$.

If this interpretation is correct, then it should also hold for plane mixing layers. As plane mixing layer experiments are often realised with low-turbulent incoming flows or even laminar incoming flows, K is lower than in high Reynolds number flows, as compound channel flows, and therefore λ_{crit} becomes smaller. Bell and Mehta (1990) and Olsen and Dutton (2002) both found indeed large-scale structures in their plane mixing layers, for which the shear parameter was respectively $\lambda = 0.25$ and $\lambda = 0.23$. The turbulence intensity of the free streams was about 0.15 % for the former and 0.8 % for the latter, which would then correspond to $K = 0.008$ and $K = 0.0015$ respectively, and therefore to a much smaller λ_{crit}.

Brown and Roshko (1974) plotted the vorticity-thickness spreading rate for plane mixing layers as a function of λ, for λ ranging from 0.1 to 1. The increase in the vorticity-thickness spreading rate with λ is quite linear without any jump. There is no threshold effect associated with λ. This could again be explained by the very low turbulent intensity with which these experiments were carried out.

By comparing two plane mixing layers for which the boundary layers on both sides of the splitter plate are either untripped (laminar) or tripped (turbulent), all other conditions being the same, Bell and Mehta (1990) showed that for the untripped case, the mixing layer width grew faster. They also noted that organised vortical structures "of scale comparable to the mixing layer thickness has been measured in the untripped case, but not in the mixing layer with the initial boundary layers tripped". The turbulent flow downstream of the splitter plate would have avoided Kelvin-Helmholtz structures to develop at this low-λ level ($\lambda = 0.25$), while they could develop for the untripped case with very low turbulence level.

In laminar inviscid plane mixing layers, the Kelvin-Helmholtz instability occurs for any velocity difference (Huerre and Rossi 1998). In a laminar viscous plane mixing layer, this seems also the case, the effect of the viscosity being just to render the small wave length more stable (Betchov and Szewczyk 1963). This supports therefore the conjecture above that there seems to be no other physical effect to hinder the formation of Kelvin-Helmholtz structures in a shear layer apart from the ambient turbulence.

The influence of ambient turbulence on large-scale structures was also observed by Gaskin et al. (2004) in the case of the plane jet: if at 0 % ambient turbulence, the jet features large-scale structures and a rapid widening, at 15 % ambient turbulence, no large-scale structures are noticeable and, after the widening of the very near-jet, the width of the jet becomes nearly constant. In the same way, Eames et al. (2011) showed that ambient turbulence has an important impact on the spreading of a wake.

7 Discussion on shear layer widening

It is known from investigations of shear layers in shallow flows that the ambient turbulence – in this case the bed-induced turbulence – does not only affect the onset of Kelvin-Helmholtz structures, but also affects, when these structures are present, the width reached by these structures and therefore by the shear layer. The influence of bed-induced turbulence on the width limitation of shear layers was investigated by a series of studies (Chu et al. 1983, 1991; Ghidaoui and Kolyshkin 1999; van Prooijen and Uijttewaal 2002; Socolofsky and Jirka 2004; Lam et al. 2016; Proust et al. 2022), which use for this aim the so-called bed-friction number S:

$$S = \frac{c_f \delta}{2h} \frac{U_0}{\Delta U} \tag{2}$$

where c_f is the bed friction coefficient, δ the shear layer width, h the water depth, U_0 the mean velocity across the shear layer, and $\Delta U = U_2 - U_1$ is the difference in velocity between the low- and high-speed side of the shear layer. The shear layer continues to widen as long as S is smaller than a critical bed friction number S_c which is on the order of 0.1 (Chu and Babarutsi 1988). On the contrary, when $S > S_c$ the shear layer does not widen any more. The bed friction number given by Eq. 2 is well defined in the case of a channel with constant water depth and roughness across the shear layer. However, for compound or composite (i.e. with a lateral variation in roughness) channels, the way to choose c_f and h is not obvious. For the following discussion, we propose therefore to define a bed friction number on each side i of the shear layer:

$$S_i = \frac{c_{f,i} \delta_i}{h_i} \frac{U_0}{\Delta U} \tag{3}$$

where δ_i, $c_{f,i}$ and h_i are the shear layer width, bed friction coefficient and water depth (the last two considered as constant) on the side i of the shear layer, the other quantities being the same as in Eq. 2 (a factor of 2 was added for the definition of S_i to take into account that only one side of the shear layer is considered). Indeed, the growth of each side of the shear layer can be independent from each other: one side can have reached a constant width whereas the other continues to widen (Dupuis et al. 2017; Proust and Nikora 2020).

The bed-friction number criterion for the convergence of the shear layer width can be reformulated in the following way: the maximal width which can be reached by a given side i of the shear layer is

$$\delta_{i,max} = 2S_c \, \lambda \, \frac{h_i}{c_{f,i}}. \tag{4}$$

This expression is the product of a proportionality factor ($2S_c \approx 0.2$), of the shear parameter λ and of a length scale, $h_i/c_{f,i}$, called the bed friction length scale after Chu and Babarutsi (1988).

By investigating vertical shear layers which develop in channel flows between a submerged canopy and the free flow above, Ghisalberti and Nepf (2004) derived the following expression for estimating the maximal penetration length of the shear layer within the canopy:

$$\delta_{\text{canopy, max}} = \frac{1}{\Omega} \gamma \frac{1}{C_D a} \tag{5}$$

where Ω is a constant close to 9, a is the frontal area per unit volume, C_D the mean drag coefficient of the roughness elements and γ is the shape function of the velocity profile (Ghisalberti and Nepd 2006), defined as $\gamma = \frac{(U_2 - U_1)^2}{U_h^2 - U_1^2}$ where U_h is the velocity at the top of the canopy. Equation 5 has therefore a form similar to Eq. 4: the product of a proportionality factor, of a parameter representing the velocity difference across the shear layer, and of a length scale, which this time is related to the canopy, $1/(C_D a)$.

In addition, Eqs. 4 and 5 can be interpreted in the same manner, namely as an energy balance, as was done by Chu et al. (1991) and Proust et al. (2022) for the bed friction number S and by Ghisalberti and Nepf (2004) for Eq. 5. In both cases, the width of the shear layer ceases to grow when a balance establishes between the production of large-scale turbulent kinetic energy (which is extracted from the time-averaged flow kinetic energy) and the energy dissipation. This dissipation is due in the first case to bed friction (Eq. 4) and in the second case to the presence of solid elements which exert a volume force on the flow (Eq. 5). These two sources of dissipation can of course be combined.

8 Conclusion

Experiments were conducted in a two-stage compound channel for different relative depths (ratio between floodplain and main channel water depth), or equivalently different values of the shear parameter λ. By means of a large-scale PIV measurement technique, the velocity field at the free surface could be recorded over a distance of six times the channel width.

For all flows, which differ both by shear parameter and Reynolds number, a shear layer can be observed, i.e. a region of high turbulent shear stress which is not due to the presence of a wall. However, two very different types of shear layer could be distinguished:

- Type 1 is characterised by the presence of large-scale quasi-periodic structures of Kelvin-Helmholtz type. This shear layer is widening in downstream direction, and located rather towards the floodplain. The large-scale structures themselves also grow downstream.
- Type 2 is characterised by the absence of quasi-periodic Kelvin-Helmholtz structures. Vortical structures are present, but these are much smaller scale, quasi-isotropic and do not grow when going downstream. The shear layer is located rather towards the main channel and it is not widening when going downstream.

Supporting the result of Proust et al. (2017), it was observed that the shear parameter λ is an effective criterion to distinguish these two shear layer types: shear layers of type 1 were observed to develop only for $\lambda > 0.3$.

This λ-criterion is proposed to be interpreted in the following way: it gives the condition for which burgeoning Kelvin-Helmholtz structures can develop and grow without being disintegrated by the ambient turbulence, i.e. by turbulent fluctuations in the surrounding of the shear layer and which stem from other turbulence sources (e.g. wall turbulence). The influence of ambient turbulence on the onset of large-scale structures was also observed in the literature for other flows, as plane mixing layers, jets and wakes.

The turbulent shear stress, when normalised by the velocity difference $U_2 - U_1$ appeared to be on the same magnitude for the two types of shear layers, except in the region $\lambda \approx 0.3$ where it is 3-4 times lower. It seems therefore that the two types of shear layer have the same efficiency to generate turbulent shear stress for a given velocity difference, apart from the λ-region close to the threshold value λ_{crit}, where the two turbulence mechanisms corresponding to the two shear layer types may be in conflict. In turn, the Reynolds number appeared to have no influence on the shear layer ability to generate turbulent shear stress.

Surprisingly, for some flows the two types of shear layer coexist side-by-side. Further research is needed to better understand this double shear layer structure.

Acknowledgements We express our gratitude to M. Ziegler and J. Ulrich for helping with the set-up of the experiments and D. Gross for helping with the data acquisition. LS received financial support through a DAAD scholarship. OE acknowledges financial support for the experimental infrastructure for these experiments through a KIT start-up grant. We thank Frédéric Moulin (IMFT) for fruitful discussions on the bed-friction number.

Author Contributions VD and OE conceptualized and conceived the experiments. LS and VD performed the experiments, the data processing and the data analysis. The results were discussed amongst all authors. VD wrote the manuscript. OE and VD edited the manuscript.

Funding Open Access funding enabled and organized by Projekt DEAL.

Data Availability The data are available upon request.

Declarations

Conflict of interests No conflicts of interest.

Ethical Approval Not applicable.

References

Bell JH, Mehta RD (1990) Development of a two-stream mixing layer from tripped and untripped boundary layers. AIAA J 28(12):2034–2042

Betchov R, Szewczyk A (1963) Stability of a shear layer between parallel streams. Phys Fluids 6(10):1391–1396

Bousmar D, Riviere N, Proust S, Paquier A, Morel R, Zech Y (2005) Upstream discharge distribution in compound-channel flumes. J Hydraul Eng 131(5):408–412

Brown GL, Roshko A (1974) On density effects and large structure in turbulent mixing layers. J Fluid Mech 64(04):775–816

Chu V, WU J, Khayat R (1983) Stability of turbulent shear flows in shallow channel. In: Proceedings XX Congress IAHR, Moscow, 1983, vol 3, pp 128–133

Chu V, Wu JH, Khayat R (1991) Stability of transverse shear flows in shallow open channels. J Hydraul Eng 117(10):1370–1388

Chu VH, Babarutsi S (1988) Confinement and bed-friction effects in shallow turbulent mixing layers. J Hydraul Eng 114(10):1257–1274

Dupuis V (2016) Experimental investigation of flows subjected to a longitudinal transition in hydraulic roughness in single and compound channels. Université de Lyon, France

Dupuis V, Proust S, Berni C, Paquier A (2017) Mixing layer development in compound channel flows with submerged and emergent rigid vegetation over the floodplains. Exp Fluids 58(4):30

Eames I, Jonsson C, Johnson P (2011) The growth of a cylinder wake in turbulent flow. J Turbul 12:N39

Epps B (2017) Review of vortex identification methods. In: 55th AIAA aerospace sciences meeting, pp 0989

Fujita I, Muste M, Kruger A (1998) Large-scale particle image velocimetry for flow analysis in hydraulic engineering applications. J Hydraul Res 36(3):397–414

Gaskin S, McKernan M, Xue F (2004) The effect of background turbulence on jet entrainment: an experimental study of a plane jet in a shallow coflow. J Hydraul Res 42(5):533–542

Ghidaoui MS, Kolyshkin AA (1999) Linear stability analysis of lateral motions in compound open channels. J Hydraul Eng 125(8):871–880

Ghisalberti M, Nepf H (2004) The limited growth of vegetated shear layers. Water Resour Res 40(7)
Ghisalberti M, Nepf H (2006) The structure of the shear layer in flows over rigid and flexible canopies. Environ Fluid Mech 6(3):277–301
Huerre P, Rossi M (1998) Hydrodynamic instabilities in open flows. Collect Alea Saclay Monogr Texts Statis Phys 1(3):81–294
Kironoto B, Graf WH (1994) Turbulence characteristics in rough uniform open-channel flow. Proc ICE-Water Maritime Energy 106(4):333–344
Lam M, Ghidaoui MS, Kolyshkin A (2016) The roll-up and merging of coherent structures in shallow mixing layers. Phys Fluids 28(9):094103
Loucks RB, Wallace JM (2012) Velocity and velocity gradient based properties of a turbulent plane mixing layer. J Fluid Mech 699:280–319
Nezu I, Nakagawa H (1993) Turbulent in open-channel flow. IAHR MonographSeries, The Netherlands
Olsen MG, Dutton JC (2002) Stochastic estimation of large structures in an incompressible mixing layer. AIAA J 40(12):2431–2438
Proust S, Nikora VI (2020) Compound open-channel flows: effects of transverse currents on the flow structure. J Fluid Mech. https://doi.org/10.1017/jfm.2019.973
Proust S, Fernandes JN, Peltier Y, Leal JB, Riviere N, Cardoso AH (2013) Turbulent non-uniform flows in straight compound open-channels. J Hydraul Res 51(6):656–667
Proust S, Fernandes JN, Leal JB, Rivière N, Peltier Y (2017) Mixing layer and coherent structures in compound channel flows: effects of transverse flow, velocity ratio, and vertical confinement. Water Resour Res 53(4):3387–3406
Proust S, Berni C, Nikora VI (2022) Shallow mixing layers over hydraulically smooth bottom in a tilted open channel. J Fluid Mech 951:A17
Sellin RHJ (1964) A laboratory investigation into the interaction between the flow in the channel of a river and that over its flood plain. La Houille Blanche 7:793–802
Socolofsky SA, Jirka GH (2004) Large-scale flow structures and stability in shallow flows. J Environ Eng Sci 3(5):451–462
Song T, Chiew Y (2001) Turbulence measurement in nonuniform open-channel flow using acoustic doppler velocimeter (adv). J Eng Mech 127(3):219–232
Stocchino A, Brocchini M (2010) Horizontal mixing of quasi-uniform straight compound channel flows. J Fluid Mech 643:425–435
van Prooijen BC, Uijttewaal WS (2002) A linear approach for the evolution of coherent structures in shallow mixing layers. Phys Fluids 14(12):4105–4114
Vella D, Mahadevan L (2005) The "cheerios effect''. Am J Phys 73(9):817–825
Weitbrecht V, Kühn G, Jirka G (2002) Large scale Piv-measurements at the surface of shallow water flows. Flow Meas Instrum 13(5–6):237–245
Yule AJ (1972) Two-dimensional self-preserving turbulent mixing layers at different free stream velocity ratios. HM Stationery Office